38th Fluid Dynamics Conference and Exhibit
23 - 26 June 2008, Seattle, Washington

AIAA 2008-3855

Detached-Eddy Simulations of a Circular Cylinder Using a Low Diffusion E-CUSP and High-Order WENO Scheme

Baoyuan Wang[*], Ge-Cheng Zha[†], Yiqing Shen [‡]
Dept. of Mechanical and Aerospace Engineering
Miami Wind^{TM}
University of Miami
Coral Gables, Florida 33124
E-mail: gzha@miami.edu

Abstract

A detached-eddy simulation (DES) of a cylinder turbulent flow using a newly developed low diffusion E-CUSP (LDE) scheme with fifth-order WENO scheme is conducted. A conservative fourth-order accuracy finite central differencing scheme is used for the viscous terms. The computed results for the baseline grid agree well with the experiment. The solution sensitivity to spanwise length is investigated. The mesh refinement is performed. The results show that the mesh refinement has a significant effect on the DES simulation.

1 Introduction

To resolve the aerodynamic non-linearity such as shock wave/turbulent boundary layer interaction and flow separation, the turbulence simulation is critical. The widely used methods for predictions of turbulent flow are based on Reynolds averaged Navier-Stokes equations (RANS). However, RANS models are not able to simulate the flow separation correctly. RANS methods intend to calculate the large scale eddies using a universal model. Large scale turbulence is affected by the flow geometry and boundary conditions and a universal model does not exist.

Large Eddy Simulation (LES) is promising to overcome the disadvantages of the RANS model. In LES, the governing equations are spatially filtered on the scale of the numerical grid. The large energy containing scales are directly simulated, and the small scale eddies, which are generally more homogeneous and universal, are modeled. The large eddies are strongly affected by the flow field geometry boundaries. Therefore the direct computation of the large eddies by LES is more accurate than the modeling of the large eddies by RANS. The effect of the unresolved small scales of motion is modeled by a subgrid-scale (SGS) model [1][2][3][4][5] or by the inherent dissipation in the numerical schemes[6][7]. Because the statistics of the small scale turbulence are more isotropic and universal, a general physical model for small scale eddies is more plausible.

---

[*] Graduate Student, AIAA Member

[†] Associate Professor, AIAA Senior Member, Director of Miami Wind^{TM}

[‡] Research Scientist, AIAA Member

However, for high Reynolds number flows such as those of transonic wings and turbo-machinery blades, to resolve the wall boundary layer, LES needs the CPU resource not much less than the Direct Numerical Simulation(DNS). This makes the LES too expensive for high Reynolds flow calculations. For engineering applications, it is not hopeful for LES to be rigorously used until in another 4 decades [8]. To overcome the intensive CPU requirement for LES, Spalart et al. developed the so called detached-eddy simulation (DES) strategy[8], which is a hybrid RANS and LES method. Near the solid surface within the wall boundary layer, the unsteady RANS model is realized. Away from the wall surface, the model automatically converts to LES. By using the RANS model near the wall, the mesh size as well as the CPU time can be tremendously reduced. The motivation of DES is that the LES is powerful in regions of massive separation and other free shear flows such as jets, but much too costly in the large area of thin wall boundary layers.

Spalart gave a grid guidance for DES in 2001[9, 10], which divides a flow domain with solid walls to Euler region, RANS region, and LES region. In the RANS region, the domain is further divided to Viscous region and Outer region. The LES region is composed of Viscous, Focus and Departure region. Spalart's DES grid guidance give sufficient grid resolution for LES region and the transition to Euler region and from RANS region. The grid size is dramatically reduced compared to the pure LES.

Even though DES concept is much newer than RANS and LES concept, its application for turbulence simulation has already achieved encouraging success as shown in the work of Tarvin et al. (1999) [11], Spalart (2001)[9, 10], Forsythe et al.(2002)[12], Viswanathan et al. [13], Squires et al.[14, 15], Hsnsen, et al. (2003)[16], Subbareddy et al. (2005) [17]. These flows calculated using DES include those for airfoils, cylinders, forbodies, base flows, etc. The results are qualitatively and quantitatively better than the solutions using RANS. DES appears to be a suitable compromise between the physical models of turbulence and CPU efficiency. In those DES applications, almost all the algorithms use 2nd order accuracy except that of Tarvin et al. (1999) [11], which employs fifth order upwind scheme for the inviscid convective terms in space.

The purpose of this paper is to develop a high order methodology of DES with shock capturing capability. A recently developed low diffusion E-CUSP scheme [18] with fifth-order WENO scheme[19, 20] is employed for the inviscid fluxes. A conservative fourth-order accuracy finite central differencing scheme is used for the viscous terms[20]. The DES strategy of Spalart[9, 10] based on Spalart-Allmaras one equation turbulence model is adopted.

2 Governing Equations

The governing equations for the flow field computation are the spatially filtered 3D general Navier-Stokes equations in generalized coordinates and can be expressed as the following:

$$\frac{\partial \mathbf{Q}'}{\partial t}+\frac{\partial \mathbf{E}'}{\partial \xi}+\frac{\partial \mathbf{F}'}{\partial \eta}+\frac{\partial \mathbf{G}'}{\partial \zeta}=\frac{1}{\mathrm{Re}}\left(\frac{\partial \mathbf{E}'_{\mathbf{v}}}{\partial \xi}+\frac{\partial \mathbf{F}'_{\mathbf{v}}}{\partial \eta}+\frac{\partial \mathbf{G}'_{\mathbf{v}}}{\partial \zeta}\right) \tag{1}$$

where Re is the Reynolds number, and

$$\mathbf{Q}'=\frac{\mathbf{Q}}{J} \tag{2}$$

$$\mathbf{E}' = \frac{1}{J}(\xi_t \mathbf{Q} + \xi_x \mathbf{E} + \xi_y \mathbf{F} + \xi_z \mathbf{G}) \tag{3}$$

$$\mathbf{F}' = \frac{1}{J}(\eta_t \mathbf{Q} + \eta_x \mathbf{E} + \eta_y \mathbf{F} + \eta_z \mathbf{G}) \tag{4}$$

$$\mathbf{G}' = \frac{1}{J}(\zeta_t \mathbf{Q} + \zeta_x \mathbf{E} + \zeta_y \mathbf{F} + \zeta_z \mathbf{G}) \tag{5}$$

$$\mathbf{E_v}' = \frac{1}{J}(\xi_x \mathbf{E_v} + \xi_y \mathbf{F_v} + \xi_z \mathbf{G_v}) \tag{6}$$

$$\mathbf{F_v}' = \frac{1}{J}(\eta_x \mathbf{E_v} + \eta_y \mathbf{F_v} + \eta_z \mathbf{G_v}) \tag{7}$$

$$\mathbf{G_v}' = \frac{1}{J}(\zeta_x \mathbf{E_v} + \zeta_y \mathbf{F_v} + \zeta_z \mathbf{G_v}) \tag{8}$$

where J is the transformation Jacobian. The variable vector $\mathbf{Q}$, and inviscid flux vectors $\mathbf{E}$, $\mathbf{F}$, and $\mathbf{G}$ are given as the following.

$$\mathbf{Q} = \begin{pmatrix} \bar{\rho} \\ \bar{\rho}\tilde{u} \\ \bar{\rho}\tilde{v} \\ \bar{\rho}\tilde{w} \\ \bar{\rho}\tilde{e} \end{pmatrix}, \mathbf{E} = \begin{pmatrix} \bar{\rho}\tilde{u} \\ \bar{\rho}\tilde{u}^2 + \bar{p} \\ \bar{\rho}\tilde{u}\tilde{v} \\ \bar{\rho}\tilde{u}\tilde{w} \\ (\bar{\rho}\tilde{e} + \bar{p})\tilde{u} \end{pmatrix}, \mathbf{F} = \begin{pmatrix} \bar{\rho}\tilde{v} \\ \bar{\rho}\tilde{v}\tilde{u} \\ \bar{\rho}\tilde{v}^2 + \bar{p} \\ \bar{\rho}\tilde{v}\tilde{w} \\ (\bar{\rho}\tilde{e} + \bar{p})\tilde{v} \end{pmatrix}, \mathbf{G} = \begin{pmatrix} \bar{\rho}\tilde{w} \\ \bar{\rho}\tilde{w}\tilde{u} \\ \bar{\rho}\tilde{w}\tilde{v} \\ \bar{\rho}\tilde{w}^2 + \bar{p} \\ (\bar{\rho}\tilde{e} + \bar{p})\tilde{w} \end{pmatrix}$$

The inviscid fluxes in generalized coordinate system are expressed as:

$$\mathbf{E}' = \begin{bmatrix} \bar{\rho}U \\ \bar{\rho}\tilde{u}U + l_x\bar{p} \\ \bar{\rho}\tilde{v}U + l_y\bar{p} \\ \bar{\rho}\tilde{w}U + l_z\bar{p} \\ (\bar{\rho}\tilde{e} + \bar{p})\,U - l_t\bar{p} \end{bmatrix}, \mathbf{F}' = \begin{bmatrix} \bar{\rho}V \\ \bar{\rho}\tilde{u}V + m_x\bar{p} \\ \bar{\rho}\tilde{v}V + m_y\bar{p} \\ \bar{\rho}\tilde{w}V + m_z\bar{p} \\ (\bar{\rho}\tilde{e} + \bar{p})\,V - m_t\bar{p} \end{bmatrix}, \mathbf{G}' = \begin{bmatrix} \bar{\rho}W \\ \bar{\rho}\tilde{u}W + n_x\bar{p} \\ \bar{\rho}\tilde{v}W + n_y\bar{p} \\ \bar{\rho}\tilde{w}W + n_z\bar{p} \\ (\bar{\rho}\tilde{e} + \bar{p})\,W - n_t\bar{p} \end{bmatrix}$$

where U, V and W are the contravariant velocities in ξ, η and ζ directions.

$$\begin{aligned} U &= l_t + \mathbf{l} \bullet \mathbf{V} = l_t + l_x\tilde{u} + l_y\tilde{v} + l_z\tilde{w} \\ V &= m_t + \mathbf{m} \bullet \mathbf{V} = m_t + m_x\tilde{u} + m_y\tilde{v} + m_z\tilde{w} \\ W &= n_t + \mathbf{n} \bullet \mathbf{V} = n_t + n_x\tilde{u} + n_y\tilde{v} + n_z\tilde{w} \end{aligned} \tag{9}$$

$\mathbf{l}$, $\mathbf{m}$, $\mathbf{n}$ are the normal vectors on ξ, η, ζ surfaces with their magnitudes equal to the elemental surface area and pointing to the directions of increasing ξ, η, ζ.

$$\mathbf{l} = \frac{\nabla\xi}{J},\ \mathbf{m} = \frac{\nabla\eta}{J},\ \mathbf{n} = \frac{\nabla\zeta}{J} \tag{10}$$

$$l_t = \frac{\xi_t}{J},\ m_t = \frac{\eta_t}{J},\ n_t = \frac{\zeta_t}{J} \tag{11}$$

$$\mathbf{E_v} = \begin{pmatrix} 0 \\ \bar{\tau}_{xx} + \sigma_{xx} \\ \bar{\tau}_{xy} + \sigma_{xy} \\ \bar{\tau}_{xz} + \sigma_{xz} \\ Q_x \end{pmatrix}, \mathbf{F_v} = \begin{pmatrix} 0 \\ \bar{\tau}_{yx} + \sigma_{yx} \\ \bar{\tau}_{yy} + \sigma_{yy} \\ \bar{\tau}_{yz} + \sigma_{yz} \\ Q_y \end{pmatrix}, \mathbf{G_v} = \begin{pmatrix} 0 \\ \bar{\tau}_{zx} + \sigma_{zx} \\ \bar{\tau}_{zy} + \sigma_{zy} \\ \bar{\tau}_{zz} + \sigma_{zz} \\ Q_z \end{pmatrix},$$

In above equations, ρ is the density, u, v, w are the Cartesian velocity components in x, y, z directions, p is the static pressure, and e is the total energy per unit mass. The overbar denotes a regular filtered variable, and the tilde is used to denote the Favre filtered variable. calculated on the baseline grid The $\bar{\tau}$ is the molecular viscous stress tensor and is estimated as:

$$\bar{\tau}_{ij} = \frac{2}{3}\tilde{\mu}\frac{\partial \tilde{u}_k}{\partial x}_k \delta_{ij} + \mu(\frac{\partial \tilde{u}_i}{\partial x_j} + \frac{\partial \tilde{u}_j}{\partial x_i}), \qquad i, j = 1, 2, 3 \tag{12}$$

The above equation is in the tensor form, where the subscript 1, 2, 3 represent the coordinates, x, y, z and the Einstein summation convention is used.

The molecular viscosity $\tilde{\mu} = \tilde{\mu}(\tilde{T})$ is determined by Sutherland law.

The σ is the subgrid scale stress tensor due to the filtering process and is expressed as:

$$\sigma_{ij} = -\bar{\rho}(\widetilde{u_i u_j} - \tilde{u}_i \tilde{u}_j) \tag{13}$$

The energy flux Q is expressed as:

$$Q_i = \tilde{u}_j(\bar{\tau}_{ij} + \sigma_{ij}) - \bar{q}_i + \Phi_i \tag{14}$$

where Φ is the subscale heat flux:

$$\Phi_i = -C_p\bar{\rho}(\widetilde{u_i T} - \tilde{u}_i \tilde{T}) \tag{15}$$

The $\bar{q}_i$ is the molecular heat flux:

$$\bar{q}_i = -\frac{C_p \tilde{\mu}}{Pr}\frac{\partial \tilde{T}}{\partial x_i} \tag{16}$$

$$\bar{\rho}\tilde{e} = \frac{\bar{p}}{(\gamma - 1)} + \frac{1}{2}\bar{\rho}(\tilde{u}^2 + \tilde{v}^2 + \tilde{w}^2) + \rho k \tag{17}$$

where γ is the ratio of specific heats, ρk is the subscale kinetic energy per unit volume.

$$\rho k = \frac{1}{2}\bar{\rho}(\widetilde{u_i u_i} - \tilde{u}_i \tilde{u}_i) = -\frac{1}{2}\sigma_{ii} \tag{18}$$

In the present calculation, the ρk in Eq.(17) is omitted based on the assumption that the effect is small.

3 Detached-Eddy Simulation

Even though above Navier-Stokes equations are given for LES, the closure of the equations will be based on the DES model suggested by Spalart et al. [8] as the following.

$$\sigma_{ij} = \mu_{DES}\left(\frac{\partial \tilde{u}_i}{\partial x_j} + \frac{\partial \tilde{u}_j}{\partial x_i} - \frac{2}{3}\frac{\partial \tilde{u}_k}{\partial x_k}\delta_{ij}\right) - \frac{2}{3}\rho k \delta_{ij} \qquad i,j = 1,2,3 \tag{19}$$

The turbulent heat flux will be evaluated as:

$$\Phi_i = C_p \frac{\mu_{DES}}{Pr_t}\frac{\partial \tilde{T}}{\partial x_i} \tag{20}$$

Where

$$\mu_{DES} = \rho\nu_t = \rho\tilde{\nu} f_{v1} \tag{21}$$

$\tilde{\nu}$ is a working variable and is determined by the following Spalart-Allmaras model[21][8][13][22]:

$$\frac{D\tilde{\nu}}{Dt} = c_{b1}\tilde{S}\tilde{\nu}\,(1 - f_{t2}) - [c_{w1}f_w - \frac{c_{b1}}{k^2}f_{t2}][\frac{\tilde{\nu}}{d}]^2 + \frac{1}{\sigma}[\nabla\cdot((\nu+\tilde{\nu})\nabla\tilde{\nu}) + c_{b2}(\nabla\tilde{\nu})^2] + f_{t1}\,(\Delta q)^2 \tag{22}$$

In generalized coordinate system, the conservative form of Eq.(22) is given as the following:

$$\begin{aligned}\frac{\partial \frac{1}{J}\rho\tilde{\nu}}{\partial t} + \frac{\partial \rho\tilde{\nu}U}{\partial \xi} + \frac{\partial \rho\tilde{\nu}V}{\partial \eta} + \frac{\partial \rho\tilde{\nu}W}{\partial \zeta} = \frac{1}{Re}\Bigg(&\frac{\partial \frac{\rho}{\sigma}\,(\nu+\tilde{\nu})\,(\mathbf{l}\bullet\nabla\tilde{\nu})}{\partial \xi} \\ .+\frac{\partial \frac{\rho}{\sigma}\,(\nu+\tilde{\nu})\,(\mathbf{m}\bullet\nabla\tilde{\nu})}{\partial \eta} + &\frac{\partial \frac{\rho}{\sigma}\,(\nu+\tilde{\nu})\,(\mathbf{n}\bullet\nabla\tilde{\nu})}{\partial \zeta} + \frac{1}{J}S_\nu\Bigg)\end{aligned} \tag{23}$$

where

$$\begin{aligned}S_\nu = \rho C_{b1}\,(1 - f_{t2})\,\tilde{S}\tilde{\nu} + \tfrac{1}{Re}\Big[&-\rho\left(C_{w1}f_w - \tfrac{C_{b1}}{\kappa^2}f_{t2}\right)\left(\tfrac{\tilde{\nu}}{d}\right)^2 \\ &+ \tfrac{\rho}{\sigma}C_{b2}\,(\nabla\tilde{\nu})^2 - \tfrac{1}{\sigma}\,(\nu+\tilde{\nu})\,\nabla\tilde{\nu}\bullet\nabla\rho\Big] + Re\left[\rho f_{t1}\,(\Delta q)^2\right]\end{aligned} \tag{24}$$

Eq.(23) is coupled with Eq.(1) when it is solved.

The eddy viscosity ν_t is obtained from:

$$\nu_t = \tilde{\nu} f_{v1} \qquad f_{v1} = \frac{\chi^3}{\chi^3 + c_{v1}^3} \qquad \chi = \frac{\tilde{\nu}}{\nu} \tag{25}$$

where ν is the molecular viscosity. The production term is:

$$\tilde{S} = S + \frac{\tilde{\nu}}{k^2 d^2}f_{v2}, \qquad f_{v2} = 1 - \frac{\chi}{1 + \chi f_{v1}} \tag{26}$$

where S is the magnitude of the vorticity. The function f_w is given by

$$f_w = g(\frac{1+c_{w3}^6}{g^6+c_{w3}^6})^{1/6}, \qquad g = r + c_{w2}(r^6 - r), \qquad r = \frac{\tilde{\nu}}{\tilde{S}k^2d^2} \tag{27}$$

The function f_{t2} is given by

$$f_{t2} = C_{t3}exp\left(-C_{t4}\chi^2\right) \tag{28}$$

and the trip function f_{t1} is

$$f_{t1} = C_{t1}g_texp\left[-C_{t2}\frac{\omega_t^2}{\Delta U^2}\left(d^2+g_t^2d_t^2\right)\right], \; g_t = min\left(0.1, \frac{\Delta q}{\omega_t \Delta x_t}\right) \tag{29}$$

where, ω_t is the wall vorticity at the wall boundary layer trip location, d is the distance to the closest wall. d_t is the distance of the field point to the trip location, Δq is the difference of the velocities between the field point and the trip location, Δx_t is the grid spacing along the wall at the trip location.

The values of the coefficients are: $c_{b1} = 0.1355, c_{b2} = 0.622, \sigma = \frac{2}{3}, c_{w1} = \frac{c_{b1}}{k^2} + (1+c_{b2})/\sigma, c_{w2} = 0.3, c_{w3} = 2, k = 0.41, c_{v1} = 7.1, c_{t1} = 1.0, c_{t2} = 2.0, c_{t3} = 1.1, c_{t4} = 2.0$.

In DES, $c_{t1} = 0$, $c_{t3} = 0$. The distance to the nearest wall, d, is replaced by $\tilde{d}$ as

$$\tilde{d} = min(d, C_{DES}\Delta) \tag{30}$$

where Δ is the largest spacing of the grid cell in all the directions.

Within the boundary layer close to walls, $\tilde{d} = d$, hence the turbulence is simulated by the RANS mode determined by the Spalart-Allmaras model[21]. Away from the boundary layer, $\tilde{d} = C_{DES}\Delta$ is most of the cases. When the production and destruction terms of the model are balanced, the length scale $\tilde{d}$ will have a Smagorinsky-like eddy viscosity and the turbulence is simulated by the LES model. Analogous to the classical LES theory, the length scale Δ is to cascade the energy to the grid size. The coefficient $C_{DES} = 0.65$ is used as set in the homogeneous turbulence[23]. The Pr_t may take the value of 0.9 within the boundary layer for RANS mode and 0.5 for LES mode away from the wall surface. Eq.(22) will be extended to generalized coordinates and will be coupled and solved together with the filtered Navier-Stokes equations, Eq.(1).

For simplicity, all the overbar and tilde in above equations will be dropped in the rest of this paper.

4 The Numerical Method

4.1 The Low Diffusion E-CUSP (LDE) Scheme[18]

The basic idea of the LDE scheme is to split the inviscid flux into the convective flux E^c and the pressure flux E^p. With the one extra equation from the S-A model for DES, the splitting is basically the same as the original scheme for the Euler equation and is straightforward. This is an advantage over the Roe scheme, for which the eigenvectors need to be derived when any extra equation is added to the governing equations.

In generalized coordinate system, the flux **E** can be split as the following:

$$\mathbf{E}' = E^c + E^p = \begin{pmatrix} \rho U \\ \rho u U \\ \rho v U \\ \rho w U \\ \rho e U \\ \rho \tilde{\nu} U \end{pmatrix} + \begin{pmatrix} 0 \\ l_x p \\ l_y p \\ l_z p \\ p\overline{U} \\ 0 \end{pmatrix} \tag{31}$$

where, U is the contravariant velocity in ξ direction and is defined as the following:

$$U = l_t + l_x u + l_y v + l_z w \tag{32}$$

$\overline{U}$ is defined as:

$$\overline{U} = l_x u + l_y v + l_z w \tag{33}$$

The convective term, E^c is evaluated by

$$E^c = \rho U \begin{pmatrix} 1 \\ u \\ v \\ w \\ e \\ \tilde{\nu} \end{pmatrix} = \rho U f^c, \ f^c = \begin{pmatrix} 1 \\ u \\ v \\ w \\ e \\ \tilde{\nu} \end{pmatrix} \tag{34}$$

let

$$C = c\left(l_x^2 + l_y^2 + l_z^2\right)^{\frac{1}{2}} \tag{35}$$

where $c = \sqrt{\gamma R T}$ is the speed of sound. Then the convective flux at interface $i + \frac{1}{2}$ is evaluated as:

$$E^c_{i+\frac{1}{2}} = C_{\frac{1}{2}}\left[\rho_L C^+ f^c_L + \rho_R C^- f^c_R\right] \tag{36}$$

where, the subscripts L and R represent the left and right hand sides of the interface.

$$C_{\frac{1}{2}} = \tfrac{1}{2}\left(C_L + C_R\right), \; C^{+} = \alpha_L^{+}\left(1 + \beta_L\right) M_L - \beta_L M_L^{+} - M_{\frac{1}{2}}^{+}$$

$$C^{-} = \alpha_R^{-}\left(1 + \beta_R\right) M_R - \beta_R M_R^{-} + M_{\frac{1}{2}}^{-}$$

$$M_L = \tfrac{U_L}{C_{\frac{1}{2}}}, \; M_R = \tfrac{U_R}{C_{\frac{1}{2}}}$$

$$\alpha_{L,R} = \tfrac{1}{2}\left[1 \pm sign\left(M_{L,R}\right)\right]$$

$$\beta_{L,R} = -max\left[0, 1 - int\left(\left|M_{L,R}\right|\right)\right]$$

$$M_{\frac{1}{2}}^{+} = M_{\frac{1}{2}} \tfrac{C_R + C_L \Phi}{C_R + C_L}, \; M_{\frac{1}{2}}^{-} = M_{\frac{1}{2}} \tfrac{C_L + C_R \Phi^{-1}}{C_R + C_L}, \; \Phi = \tfrac{\left(\rho C^2\right)_R}{\left(\rho C^2\right)_L}$$

$$M_{\frac{1}{2}} = \beta_L \delta^{+} M_L^{-} - \beta_R \delta^{-} M_R^{+}$$

$$M_{L,R}^{\pm} = \pm\tfrac{1}{4}\left(M_{L,R} \pm 1\right)^2$$

$$\delta^{\pm} = \tfrac{1}{2}\left\{1 \pm sign\left[\tfrac{1}{2}\left(M_L + M_R\right)\right]\right\}$$

The pressure flux, E^p is evaluated as the following

$$E^p_{i+\frac{1}{2}} = \begin{pmatrix} 0 \\ \mathcal{P}^{+} p\, l_x \\ \mathcal{P}^{+} p\, l_y \\ \mathcal{P}^{+} p\, l_z \\ \frac{1}{2} p\left[\overline{U} + \overline{C}_{\frac{1}{2}}\right] \\ 0 \end{pmatrix}_L + \begin{pmatrix} 0 \\ \mathcal{P}^{-} p\, l_x \\ \mathcal{P}^{-} p\, l_y \\ \mathcal{P}^{-} p\, l_z \\ \frac{1}{2} p\left[\overline{U} - \overline{C}_{\frac{1}{2}}\right] \\ 0 \end{pmatrix}_R \tag{37}$$

The contravariant speed of sound $\overline{C}$ in the pressure vector is consistent with $\overline{U}$. It is computed based on C as the following,

$$\overline{C} = C - l_t \tag{38}$$

The use of $\overline{U}$ and $\overline{C}$ instead of U and C in the pressure vector to take into account of the grid speed so that the flux will transit from subsonic to supersonic smoothly. When the grid is stationary, $l_t = 0$, $\overline{C} = C$, $\overline{U} = U$.

The pressure splitting coefficient is:

$$\mathcal{P}^{\pm}_{L,R} = \frac{1}{4}\left(M_{L,R} \pm 1\right)^2 \left(2 \mp M_L\right) \tag{39}$$

The LDE scheme can capture shock and contact surface discontinuities as accurately as the Roe scheme. However, it is simpler and more CPU efficient than the Roe scheme due to no matrix operation.

4.2 The Fifth-Order WENO Scheme

The interface flux, $E_{i+\frac{1}{2}} = E(Q_L, Q_R)$, is evaluated by determining the conservative variables Q_L and Q_R using fifth-order WENO scheme[20]. For example,

$$(Q_L)_{i+\frac{1}{2}} = \omega_0 q_0 + \omega_1 q_1 + \omega_2 q_2 \tag{40}$$

where

$$\begin{aligned} q_0 &= \tfrac{1}{3}Q_{i-2} - \tfrac{7}{6}Q_{i-1} + \tfrac{11}{6}Q_i \\ q_1 &= -\tfrac{1}{6}Q_{i-1} + \tfrac{5}{6}Q_i + \tfrac{1}{3}Q_{i+1} \\ q_2 &= \tfrac{1}{3}Q_i + \tfrac{5}{6}Q_{i+1} - \tfrac{1}{6}Q_{i+2} \end{aligned} \tag{41}$$

$$\omega_k = \frac{\alpha_k}{\alpha_0 + \ldots + \alpha_{r-1}} \tag{42}$$

$$\begin{aligned} &\alpha_k = \tfrac{C_k}{\epsilon + IS_k},\ k = 0, \ldots, r-1 \\ &C_0 = 0.1,\ C_1 = 0.6,\ C_2 = 0.3 \\ &IS_0 = \tfrac{13}{12}\left(Q_{i-2} - 2Q_{i-1} + Q_i\right)^2 + \tfrac{1}{4}\left(Q_{i-2} - 4Q_{i-1} + 3Q_i\right)^2 \\ &IS_1 = \tfrac{13}{12}\left(Q_{i-1} - 2Q_i + Q_{i+1}\right)^2 + \tfrac{1}{4}\left(Q_{i-1} - 4Q_i + 3Q_{i+1}\right)^2 \\ &IS_2 = \tfrac{13}{12}\left(Q_i - 2Q_{i+1} + Q_{i+2}\right)^2 + \tfrac{1}{4}\left(Q_i - 4Q_{i+1} + 3Q_{i+2}\right)^2 \end{aligned} \tag{43}$$

where, ϵ is originally introduced to avoid the denominator becoming zero and is supposed to be a very small number. In [20], it is observed that IS_k will oscillate if ϵ is small and also shift the weights away from the optimum values in the smooth region. The higher the ϵ values, the closer the weights approach the optimum weights, C_k, which will give the symmetric evaluation of the interface flux with minimum numerical dissipation. When there are shocks in the flow field, ϵ can not be too large to maintain the sensitivity to shocks. In [20], $\epsilon = 10^{-2}$ is recommended for the transonic flow with shock waves. In this paper, since there is no shock in the flow, the $\epsilon = 0.3$ is used.

The viscous terms are discretized by a conservative fourth-order accurate finite central differencing scheme developed by Shen et al[20].

4.3 Implicit Time Integration

The time dependent governing equations are solved using dual time stepping method suggested by Jameson[24]. To achieve high convergence rate, the implicit pseudo time marching scheme is used with the unfactored Gauss-Seidel line relaxation. The physical temporal term is discretized implicitly using a three point, backward differencing as the following (The prime is omitted hereafter for simplicity):

$$\frac{\partial \mathbf{Q}}{\partial t} = \frac{\mathbf{3Q^{n+1} - 4Q^{n} + Q^{n-1}}}{2\Delta t} \tag{44}$$

where $n-1$, n and $n+1$ are three sequential time levels, which have a time interval of Δt. The first-order Euler scheme is used to discretize the pseudo temporal term. The semi-discretized equations of the governing equations are finally given as the following:

$$\left[\left(\frac{1}{\Delta\tau} + \frac{1.5}{\Delta t}\right) I - \left(\frac{\partial R}{\partial \mathbf{Q}}\right)^{n+1,m}\right] \delta\mathbf{Q^{n+1,m+1}} = \mathbf{R^{n+1,m}} - \frac{\mathbf{3Q^{n+1,m} - 4Q^{n} + Q^{n-1}}}{\mathbf{2\Delta t}} \tag{45}$$

where the $\Delta\tau$ is the pseudo time step, R is the net flux evaluated on a grid point using the fifth-order WENO scheme and the fourth-order central differencing scheme[20].

5 Results and Discussion

In this study, the flow around a cylinder at a Reynolds number 3900 is calculated using DES. The Mach number is 0.2. The spanwise length is πD, where D is the cylinder diameter. The dimensions of the baseline grid are ($121 \times 81 \times 33$) (see Fig. 1 and Fig. 2). The computation is conducted on an MPI based computer cluster composed of 200 Intel Xeon 5150 processors with the floating calculation speed of 2.66Ghz.

A non-dimensional time step of 0.01 was used for the cases. The non-dimensional time is defined as $\bar{t} = \frac{t}{D/U_\infty}$. The computation begins with a uniform flow field. All the results are time-averaged from $\bar{t} = 100$ to 300.

Fig. 3 shows the mean pressure coefficients on the cylinder surface. For $Re = 3900$, only the coefficient of back pressure (C_p at $\theta = 180°$) is available . The computed mean pressure coefficient agrees very well with the experiment at $0 \leq \theta \leq 60°$. The present result using baseline grid is better than the LES result of Kasliwal et al[25] in this region. In the region of $\theta = 60° \sim 180°$, the computed pressure lies among the experimental results.

Fig. 4 is the averaged mean streamwise velocity on the centerline in the wake of the cylinder. The present result agrees better with the experiment[26] than those of LES [27, 25] conducted by Kravchenko-Moin and Kasliwal et al.

Fig. 5 through Fig. 7 show the Reynolds stress components located at $x/D = 1.54$ plane. The computed streamwise Reynolds stress ($\overline{u'u'}$) is quite symmetric about the center line, whereas the experiment[28] has asymmetric profile. The computed ($\overline{u'u'}$) agrees well with the experiment except it does not reach the asymmetric high peak.

The computed shear Reynolds stress component ($\overline{u'v'}$) in Fig. 6 under-predicts the amplitude of the peaks measured in the experiment. Fig. 7 also shows that the peak of the lateral Reynolds stress ($\overline{v'v'}$) is under predicted. However, all the present results are significantly better than the LES results of Rizzetta et al[29] which use 6-order compact scheme with mesh dimensions of $199 \times 197 \times 53$ as shown from Fig. 5∼ 7.

Fig. 8 and Fig. 9 plot the averaged mean streamwise velocity and mean crossflow velocity at three streamwise locations, $x/D = 1.06$, $x/D = 1.54$ and $x/D = 2.02$. The present results agree well with the computed results of Kravchenko-Moin[27] and Kasliwal et al[25].

To investigate the solution sensitivity to spanwise length, the cylinder with spanwise length doubled to $2\pi D$ is calculated. The grid density is the same as the baseline grid. Fig. 10 through Fig. 14 indicate that the spanwise length has only a small effect on the computed results. The computed surface pressure is nearly identical to the baseline results. For the $2\pi D$ spanwise length, the computation gives slightly lower minimum mean streamwise velocity in the wake region. There is also little difference for the Reynolds stress component predicted with $2\pi D$ spanwise length.

The mesh refinement is also performed in this study. The dimensions of the baseline grid are increased by 1.5 times to ($181 \times 121 \times 49$). The grid is divided into 12 blocks for parallel computation. The mesh refinement has a significant effect on the computed results. The clear difference between the refined and baseline mesh is that the refined mesh has larger vortex shedding area. Fig. 15 and Fig. 16 show the contours of the averaged mean vorticity magnitude of the baseline grid and refined grid respectively. Both display the symmetry of the mean flow field after a long time average. The refined grid predicts a larger recirculation zone behind the cylinder. Fig. 10 shows that the mean pressure distribution is raised up in the region $\theta = 60^\circ \sim 180^\circ$ and matches closer with the experiment of Reynolds number 3000. The streamwise velocity distribution is shifted away from the measurement value as shown in Fig. 11. The computed shear Reynolds stress components are sharply reduced and are closer to the LES results of Rizzetta et al.

Fig. 17 shows the contours of the instantaneous vorticity magnitude at $\bar{t} = 300$. The refined mesh catches more small scale vortex structures. Fig. 18 shows a 3D instantaneous vorticity magnitude of the $2\pi D$ cylinder at $\bar{t} = 300$. It indicates that DES resolves some small vortex structures.

6 Conclusions

A DES methodology is developed with low diffusion E-CUSP scheme [18] and fifth-order WENO scheme. A fully conservative fourth-order central differencing scheme is used for the viscous terms. For the baseline grid of $121 \times 81 \times 33$ with πD spanwise length, the computed surface pressure and velocity in the wake region agree well with the experiment. The computed Reynolds stress are also in good agreement with the experiment except that the peak values are some what under predicted. To minimize the numerical dissipation, the ϵ value of 0.3 in the WENO scheme is used.

The study indicates that the spanwise length of πD is sufficient. Doubling the spanwise length yields little difference of the results. The computation of mesh refinement indicates that DES is significantly affected by grid size. The clear difference is that the vortex shedding region is increased when the mesh is refined. The increased recirculation zone hence changes the mean values of the flow field.

7 Acknowledgment

This work is supported by AFOSR Grant F49620-03-1-0253 monitored by Fariba Fahroo and by Miami Wind^{TM} at University of Miami.

References

[1] J. Smagorinsky, "General Circulation Experiments with the Primitive Equations, I. The Basic Experiment," *Monthly Weather Review*, vol. 91, pp. 99–164, 1963.

[2] D. Lilly, "The Presentation of Small-Scale Turbulent in Numerical Simulation Experiments," *IBM Scientific Computing Symp. on Environmental Sciences*, p. 195, 1967.

[3] M. Germano, U. Piomeli, P. Moin, and W. Cabot, "A Dynamic Subgrid-scale Eddy Viscosity Model," *Physics of Fluids A*, vol. 3, pp. 1760–1765, July 1991.

[4] U. Piomeli, W. Cabot, P. Moin, and S. Lee, "Subgrid Scale Backscatter in Turbulent and Transitional Flows," *Physics of Fluids A*, vol. 3, pp. 1766–1771, July 1991.

[5] J. Deardorff, "A Numerical Study of Three Dimensional Turbulent Channel Flow at Large Reynolds Numbers," *Journal of Fluid Mechanics*, vol. 41, pp. 453–480, 1970.

[6] T. Kawamura and K. Kuwahara, "Computation of High Reynolds Number Flow Around a Circular Cylinder with Surface Roughness." AIAA Paper-84-0340, 1984.

[7] F. Grinstein, "Dynamics of Coherent Structures and Transition to Turbulence in Free Square Jet." AIAA Paper-96-0781, 1978.

[8] P. Spalart, W.-H. Jou, M. Strelets, and S. Allmaras, "Comments on the Feasibility of LES for Wings, and on a Hybrid RANS/LES Approach." Advances in DNS/LES, 1st AFOSR Int. Conf. on DNS/LES, Greyden Press, Columbus, H., Aug. 4-8, 1997.

[9] P. R. Spalart, "Young-Person's Guide to Detached-Eddy Simulation Grids." NASA/CR-2001-211032, 2001.

[10] P. R. Spalart, "Topics in Detached-Eddy Simulation."

[11] A. Tarvin, M. Shur, M. Strelets, and P. Spalart, "Detached-Eddy Simulations Past a Circular Cylinder," *Flow Turbulence and Combustion*, vol. 63, 1999.

[12] J. R. Forsythe, K. A. Hoffmann, and K. D. Cummings, R. M. Squires, "Detached-Eddy Simulations with Compressibility Corrections Applied to Supersonic Axisymmetric Base Flow," *Journal of Fluids Engineering*, vol. 124, 2002.

[13] A. Viswanathan, K. Klismith, J. Forsythe, and K. D. Squires, "Detached-Eddy Simulation around a Forebody at High Angle of Attack." AIAA-2003-0263, 2003.

[14] K. D. Squires, "Detached-Eddy Simulation: Current Status and Perspectives."

[15] K. D. Squires, J. R. Forsythe, and P. R. Spalart, "Detached-Eddy Simulation of the Seperated Flow Around a Forebody Cross-Section."

[16] R. P. Hansen and J. R. Forsythe, “Large and Detached Eddy Simulation of a Circular Cylinder Using Unstructured Grids.” AIAA Paper 2003-0775, Jan. 2003.

[17] P. Subbareddy and G. V. Candler, “Numerical Investigations of Supersonic Base Flows Using DES.” AIAA Paper 2005-0886, Jan. 2005.

[18] G.-C. Zha, Y. Shen, and B. Wang, “Calculation of Transonic Flows Using WENO Method with a Low Diffusion E-CUSP Upwind Scheme.” AIAA Paper 2008-0745, 46th AIAA Aerospace Sciences Meeting, Reno, NV, Jan. 2008.

[19] C.-W. Shu, “Essentially Non-Oscillatory and Weighted Essentially Schemesfor Hyperbolic Conservation Laws.” NASA/CR-97-206253, 1997.

[20] Y.-Q. Shen, B.-Y. Wang, and G.-C. Zha, “Implicit WENO Scheme and High Order Viscous Formulas for Compressible Flows .” AIAA Paper 2007-4431, 2007.

[21] P. Spalart and S. Allmaras, “A One-equation Turbulence Model for Aerodynamic Flows.” AIAA-92-0439, 1992.

[22] R. P. Hansen and J. Forsythe, “Large and Detached Eddy Simulation of a Circular Cylinder Using Unstructured Grids.” AIAA-2003-0775, 2003.

[23] M. Shur, P. Spalart, M. Strelets, and A. Travin, “Detached-Eddy Simulation of an Airfoil at High Angle of Attack”, 4th Int. Symp. Eng. Turb. Modelling and Measurements, Corsica.” May 24-26, 1999.

[24] A. Jameson, “Time Dependent Calculations Using Multigrid with Application to Unsteady Flows past Airfoils and Wings.” AIAA Paper 91-1596, 1991.

[25] A. Kasliwal, K. Ghia, U. Ghia , “ Higher-order accurate solution for flow past a circular cylinder at $Re = 13,4000$.” AIAA-2005-1123, 43rd AIAA Aerospace Sciences Meeting and Exhibit, Reno, Nevada,10-13 Jan., 2005.

[26] A. Krothapalli, C. Shih, and L. Lourenco, “ The near wake of a circular cylinder at $0.3 < M_\infty < 0.6$: a PIV study .” 32nd Aero Sciences Meeting and Exhibit, AIAA Paper 94-0063, 1994.

[27] G. Kravchenko, P. Moin , “ Numerical studies of flow over a circular cylinder at $Re_D = 3900$,” *Phys.Fluids* , vol. 12, pp. 403–417, 2000.

[28] L.M. Lourenco, C. Shih , “ Characteristics of the plane turbulent near wake of a circular cylinder, A particle image velocity study .” private communication by Beaudan and Moin (data taken from[27]), 1993.

[29] D.P. Rizzetta, M.R. Visbal, G.A. Blaisdell, “ A time-implicit high-order compact differencing and flitering scheme for Large-eddy simulation ,” *Int.J.Numer.Meth.Fluids* , vol. 42, pp. 665–693, 2003.

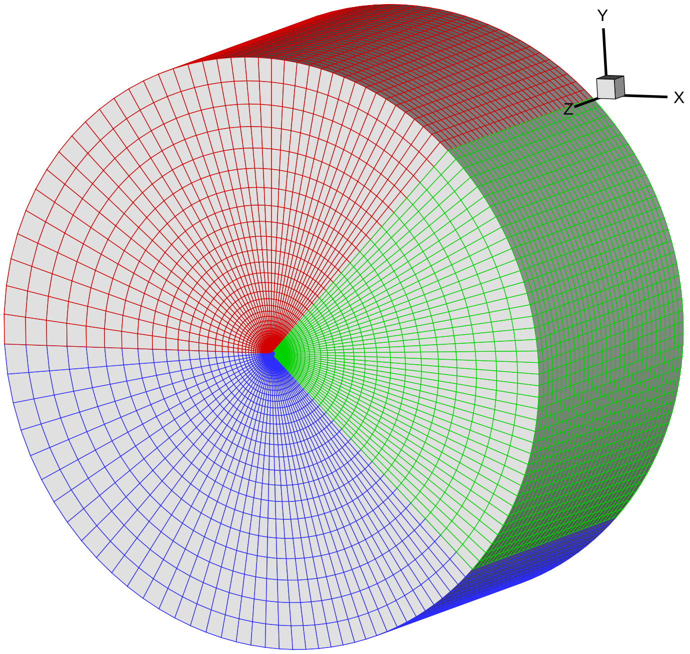

Figure 1: The computational grid of cylinder

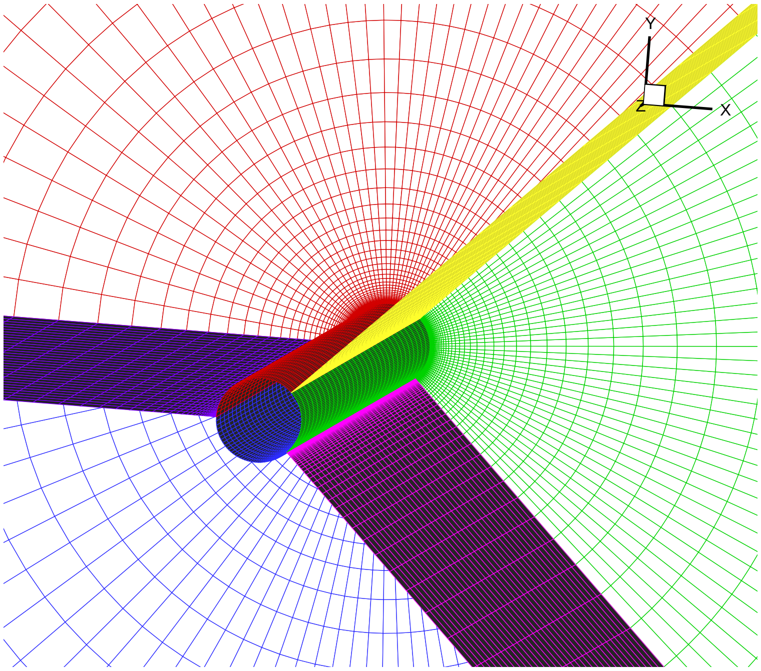

Figure 2: Close-up view of the computational grid

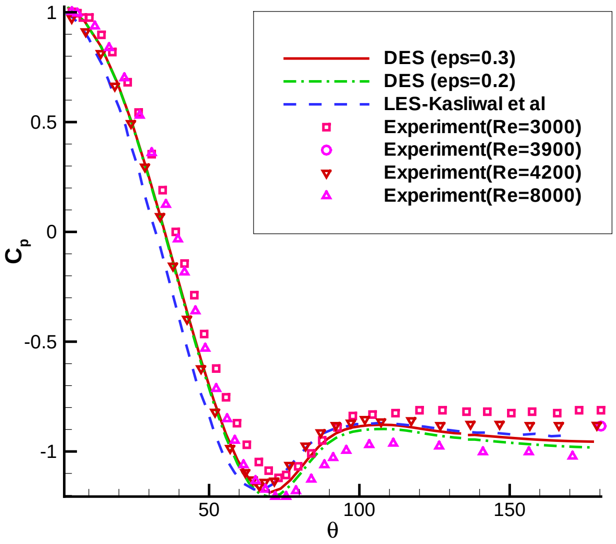

Figure 3: Mean pressure coefficient variation on the surface of the cylinder

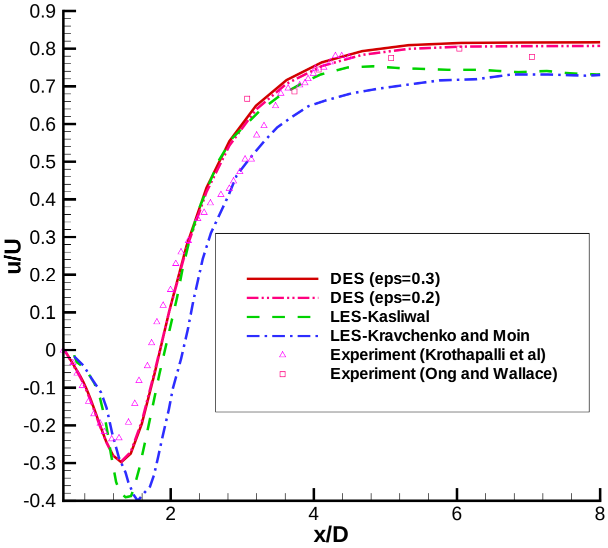

Figure 4: Streamwise velocity in the wake at y/D=0

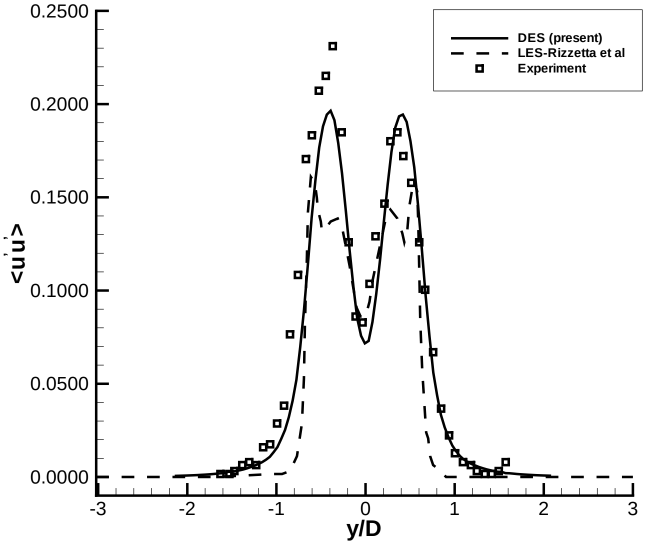

Figure 5: Streamwise Reynolds stress at x/D=1.54

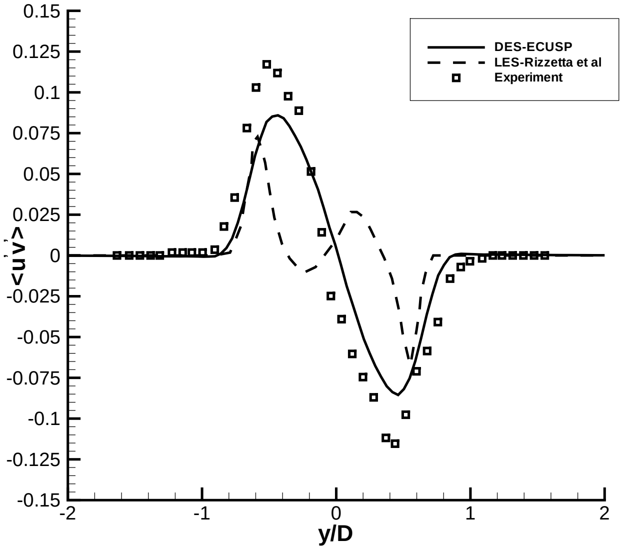

Figure 6: Shear Reynolds stress at x/D=1.54

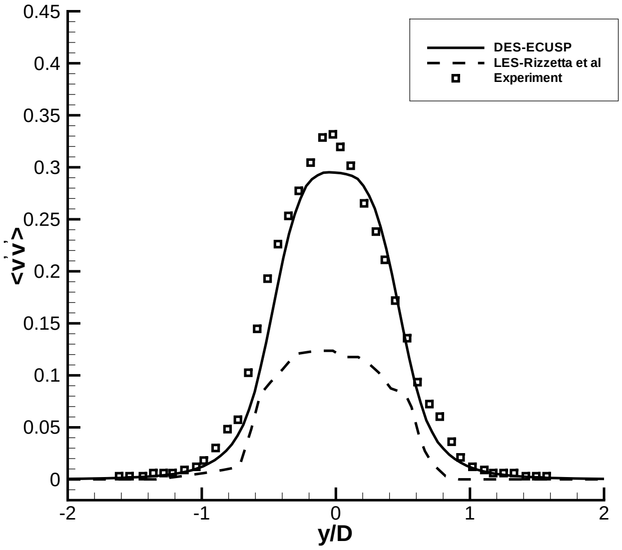

Figure 7: Lateral Reynolds stress at x/D=1.54

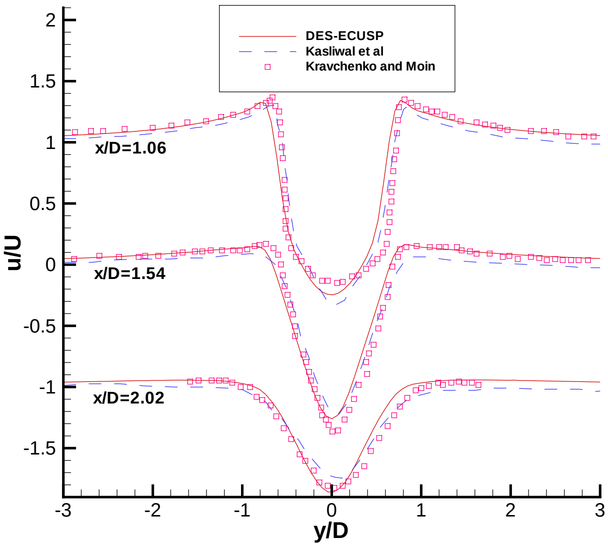

Figure 8: Mean streamwise velocity profiles in the wake

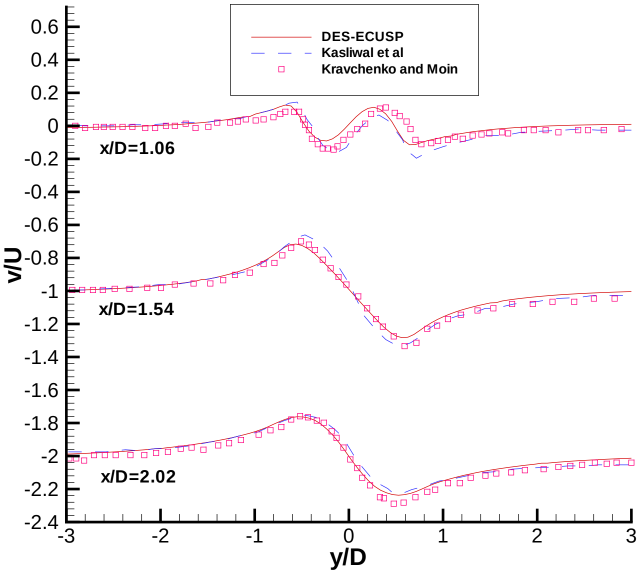

Figure 9: Mean crossflow velocity profiles in the wake

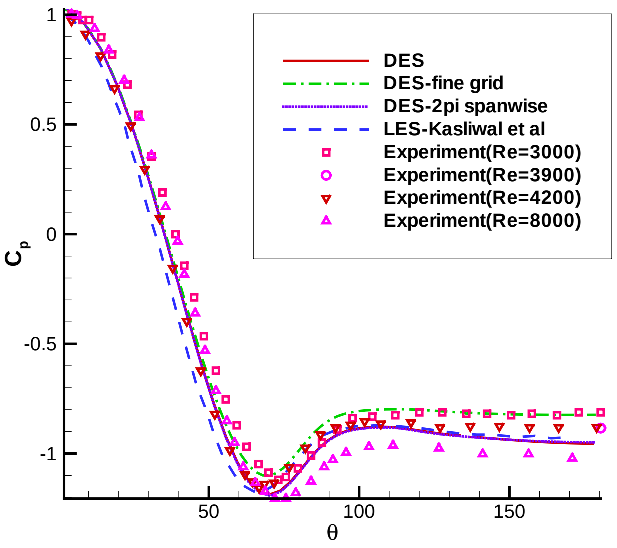

Figure 10: Mean pressure coefficient variation on the surface of the cylinder

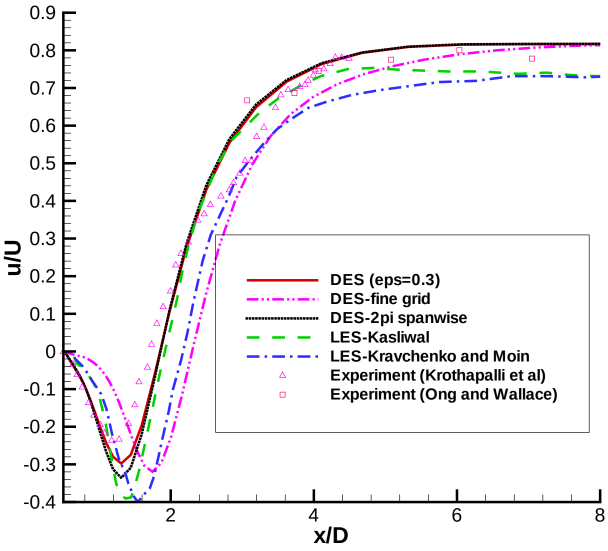

Figure 11: Streamwise velocity in the wake at y/D=0

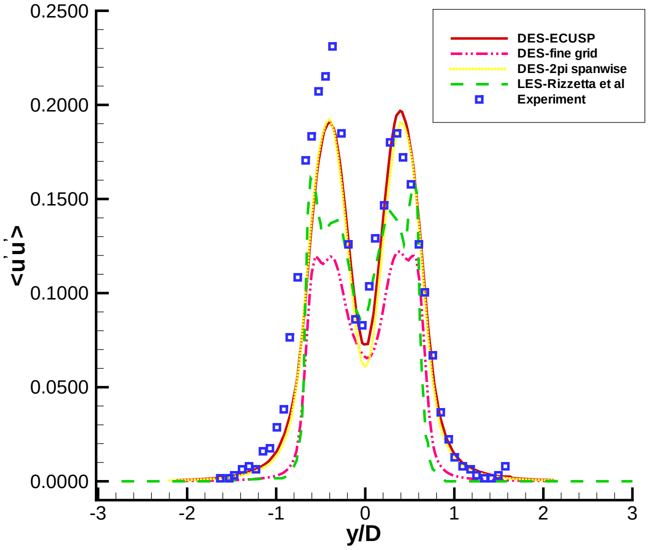

Figure 12: Streamwise Reynolds stress at x/D=1.54

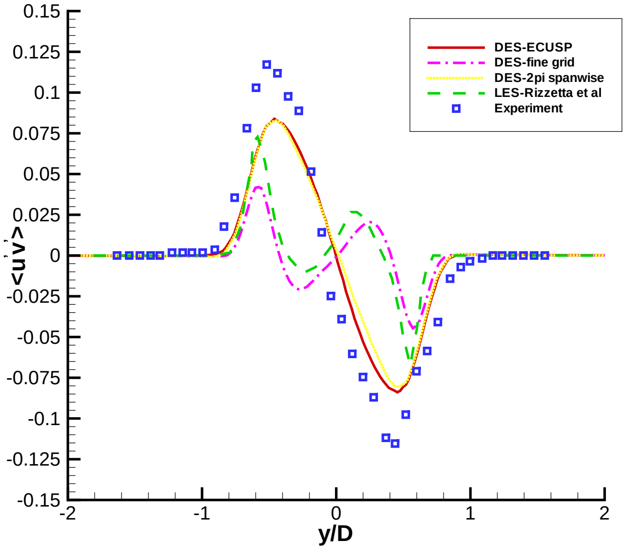

Figure 13: Shear Reynolds stress at x/D=1.54

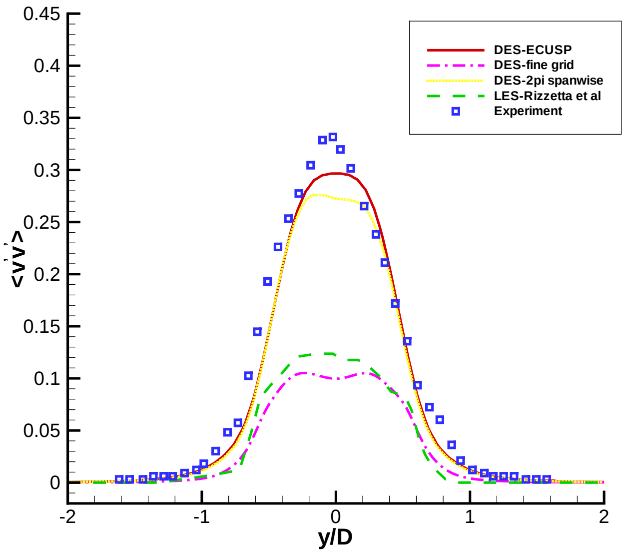

Figure 14: Lateral Reynolds stress at x/D=1.54

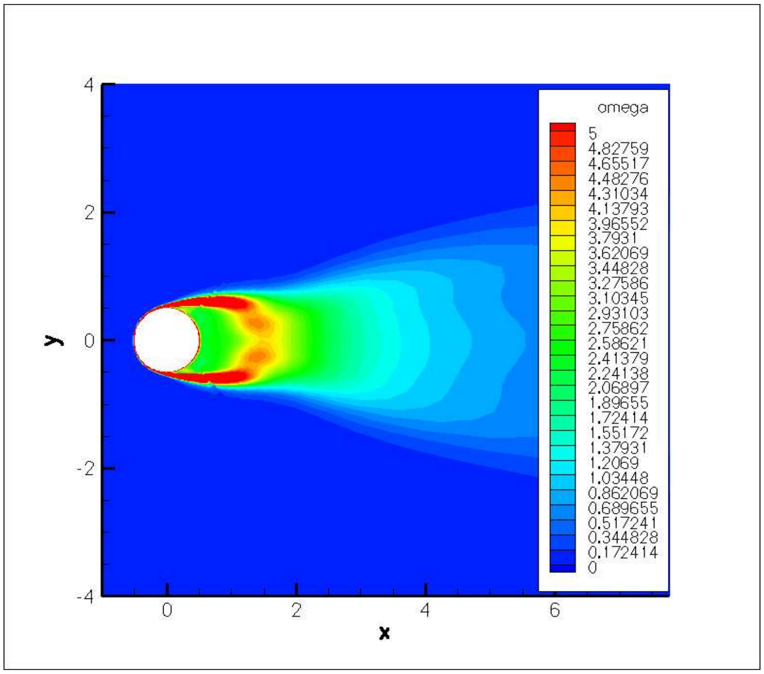

Figure 15: Contours of mean vorticity calculated on the baseline grid

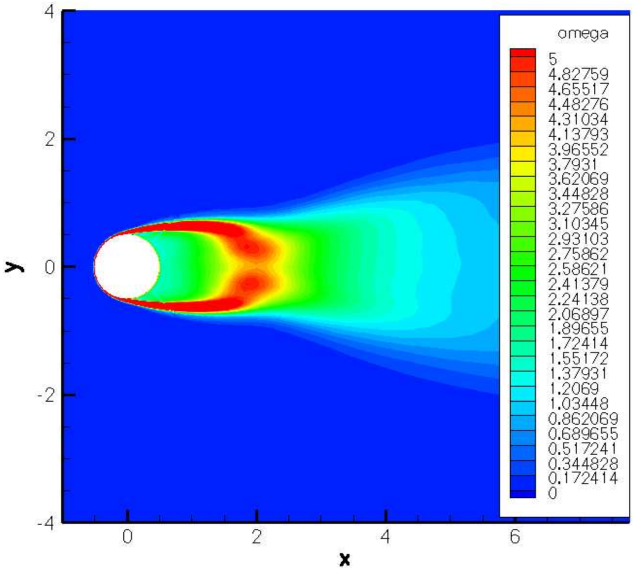

Figure 16: Contours of mean vorticity calculated on the refined grid

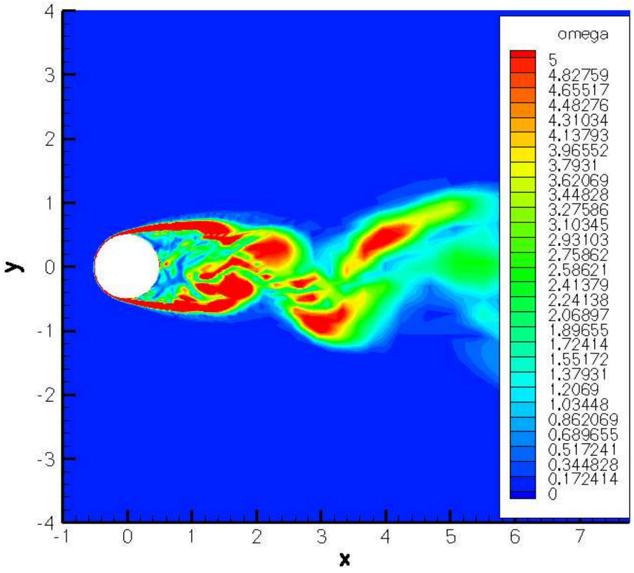

Figure 17: Contours of instantaneous vorticity at t=300T

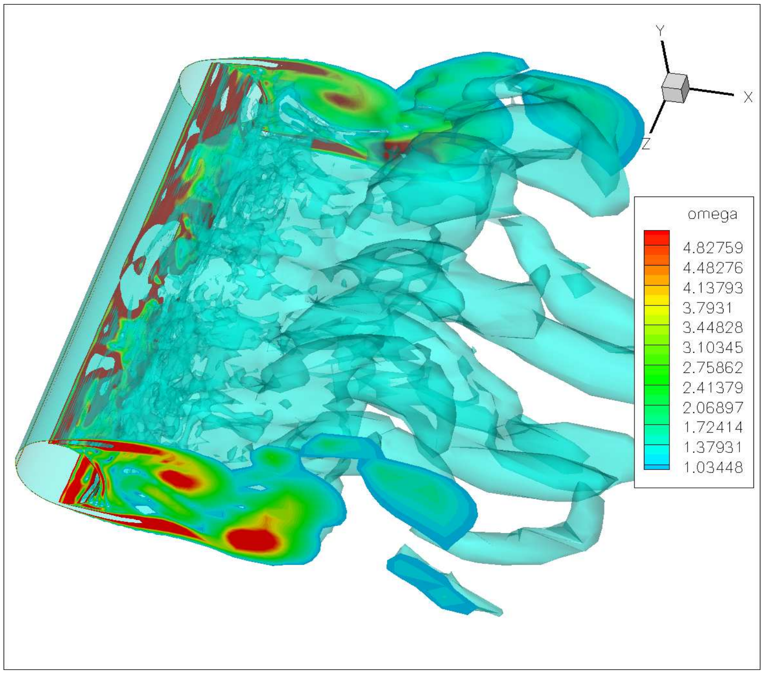

Figure 18: Contours of instantaneous vorticity at t=300T